Journal of Colloid and Interface Science 545 (2019) 330–339

Contents lists available at ScienceDirect

Journal of Colloid and Interface Science

journal homepage: www.elsevier.com/locate/jcis

Regular Article

Mucin adsorption on vaterite $CaCO_3$ microcrystals for the prediction of mucoadhesive properties

Nadezhda G. Balabushevich [a], Ekaterina A. Kovalenko [a], Elena V. Mikhalchik [b], Lyubov Y. Filatova [a], Dmitry Volodkin [a,c], Anna S. Vikulina [c,d,*]

[a] Lomonosov Moscow State University, Department of Chemistry, Leninskiye Gory 1-3, 119991 Moscow, Russia
[b] Federal Research and Clinical Centre of Physical-Chemical Medicine, Malaya Pirogovskaya 1A, 119992 Moscow, Russia
[c] Nottingham Trent University, School of Science and Technology, Clifton Lane, NG11 8NS Nottingham, UK
[d] Fraunhofer Institute for Cell Therapy and Immunology, Branch Bioanalytics and Bioprocesses, Am Mühlenberg 13, 14476 Potsdam-Golm, Germany

GRAPHICAL ABSTRACT

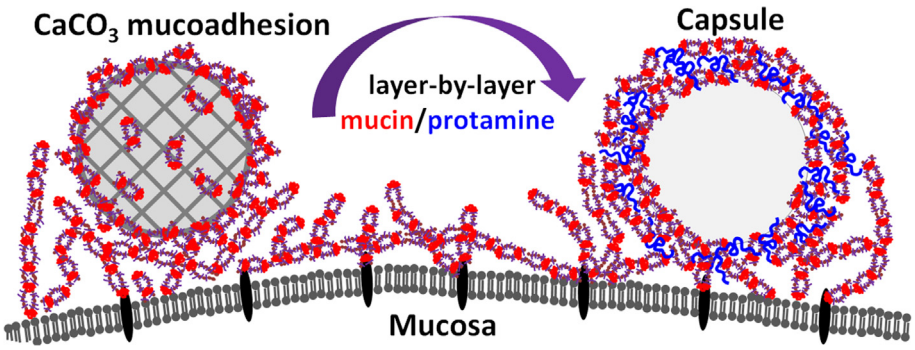

ARTICLE INFO

Article history:
Received 7 January 2019
Revised 12 March 2019
Accepted 13 March 2019
Available online 14 March 2019

Keywords:
Desialated mucin
Mucoadhesion
Layer-by-layer
Multilayer
Protamine

ABSTRACT

Porous vaterite $CaCO_3$ crystals are widely used as containers for drug loading and as sacrificial templates to assemble polymer-based nano- and micro-particles at mild conditions. Special attention is paid nowadays to mucosal delivery where the glycoprotein mucin plays a crucial role as a main component of a mucous. In this work mucoadhesive properties of vaterite crystals have been tested by investigation of mucin binding to the crystals as a function of (i) time, (ii) glycoprotein concentration, (iii) adsorption conditions and (iv) degree of mucin desialization. Mucin adsorption follows Bangham equation indicating that diffusion into crystal pores is the rate-limiting step. Mucin strongly binds to the crystals ($\Delta G = -35 \pm 4$ kJ mol^{-1}) via electrostatic and hydrophobic interactions forming a gel and thus giving the tremendous mucin mass content in the crystals of up to 16%. Despite strong intermolecular mucin-mucin interactions, pure mucin spheres formed after crystal dissolution are unstable. However, introduction of protamine, actively used for mucosal delivery, makes the spheres stable via additional electrostatic bonding. The results of this work indicate that the vaterite crystals are extremely promising carriers for mucosal drug delivery and for development of test-systems for the analysis of the mucoadhesion.

* Corresponding author at: Fraunhofer Institute for Cell Therapy and Immunology, Branch Bioanalytics and Bioprocesses, Am Mühlenberg 13, 14476 Potsdam-Golm, Germany.

E-mail addresses: sholina-katya@mail.ru (E.A. Kovalenko), lemik2007@yandex.ru (E.V. Mikhalchik), dmitry.volodkin@ntu.ac.uk (D. Volodkin), anna.vikulina@izi-bb.fraunhofer.de (A.S. Vikulina).

https://doi.org/10.1016/j.jcis.2019.03.042
0021-9797/

1. Introduction

Biodegradable and biocompatible $CaCO_3$ crystals are actively used as the templates for the preparation of polymer particles for various applications [1–4] and also directly utilized as containers for loading of biologically active substances (BAS) of various nature [5–9]. Among all the polymorphs of $CaCO_3$, special attention is paid to the vaterite crystals [4]. Conventionally, simple methods are employed for the fabrication of the vaterite crystals. These crystals are microspheres of the size that can vary from hundreds of nanometers up to tens of micrometers. The main advantage of the crystals is a highly porous internal structure offering a large surface. The change of the size of nanocrystallines that form microcrystals can be controlled via variation of crystal preparation conditions that leads to a change in the pore size and the adsorption capacity of macromolecules with different molecular weights [10]. The inclusion of both high-molecular-weight biomolecules (enzymes, proteins, hormones, DNA, RNA) and low-molecular-weight soluble and insoluble substances (antibiotics, anti-cancer agents, etc.) has been reported [4,5,11–22]. Varying the composition of preparation medium and using various biopolymers or lipids as additives gives an option to suppress the recrystallization of the vaterite crystals into thermodynamically more stable modifications and thus regulate the release of BAS [20,23–25]. Different approaches for the employment of nano- and micro-sized vaterite crystals for delivery of various BASs have been discussed [21], including mucosal delivery through mucosal surfaces [8,26].

Mucoadhesive drug delivery systems [27,28] include buccal, oral, vaginal, rectal, nasal and ocular delivery systems [29–32]. Mucous surfaces of various organs differ in their structure, thickness and composition [28]. Mucins are essential and most important component of mucus which mainly determines the transit and protective properties of mucous surfaces [33–35]. Mucins are broadly classified as two types - secreted mucins and membrane bound mucins.

Mucins are extracellular glycoproteins of large molecular weights of 0.5–20 MDa. Both membrane bound mucins, and secreted mucins [36] share many common features. They consist of ca 80% of carbohydrates which are mainly *N*-acetylgalactosamine, *N*-acetylglucosamine, fucose, galactose, and *N*-acetylneuraminic (sialic) acid. These carbohydrates are oligosaccharide chains consisting of 5–15 monomers. Oligosaccharides are attached to the protein core via covalent O-glycosidic bonds with the side hydroxyl groups of serine and threonine. This structure ensures so called bottle-brush configuration about the protein core. Remaining up to 20% of the molecular mass of mucin consists of the protein core that is arranged into two distinct regions. A central glycosylated region is comprised of a large number of tandem repeats of amino acid sequences in which up to >60% are serine, threonine and proline (STP repeats). Second type of the protein regions is located at the amino- and carboxy- terminals, and sometimes interspersed between the STP-repeats. The amino acid composition of these regions is more consistent with a structure of globular proteins in which there is a relatively little number of O-glycosylation and a few *N*-glycosylation sites and a high proportion of cysteine (>10%). The formation of S-S disulphide bonds between cysteines in these cysteine-rich domains leads to a subsequent polymerization of mucin dimers to form multimers (Fig. 1) [33].

Drug delivery systems that are used for mucosal delivery should (i) have mucoadhesive properties, namely the ability to be bonded and retained on the mucous surface for a long time, mainly through interaction with mucin, (ii) ensure prolonged release of BAS, and then (3) be detached of the mucosa causing minimal damage to it [27,37,38]. Mucoadhesive properties of drug delivery systems should also increase the bioavailability of the BASs included in them [27]. Mucoadhesive drug delivery systems are designed for both local delivery and for systemic administration via BAS penetration through mucous surfaces and entering the blood circulatory system.

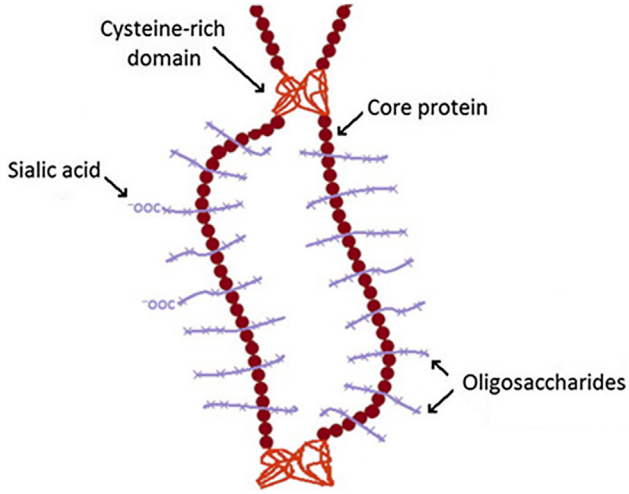

Fig. 1. Schematic structure of mucin glycoproteins.

All new mucoadhesive delivery systems are to be pre-examined and tested. At present, an impressive arsenal of various biological (including tests on model animals) as well as physical and chemical methods are in use for analysis of mucoadhesive properties, both polymers and delivery systems based on nano- or micro-particles [38]. The majority of these methods is based on the use of specific, complex and expensive equipment. Methods of analysis using mucous surfaces are widely applied [37]. However, mucous surfaces isolated from living organisms are characterized by fragility, heterogeneity, limited shelf life (2–3 h) and change of the properties during freezing that result in reduced reproducibility in experiments.

Meanwhile, mucoadhesive properties of different nano- and micro-particles can be analyzed via adsorption of commercial mucins [39]. This adsorption method is relatively simple, although it is mentioned in a number of works that the results of the analysis can be influenced by the method of isolation and purification of mucin [34,40]. The decrease of mucin concentration in solution can easily be determined by conventional methods of glycoprotein detection [34]. It was shown that the method of adsorption is highly reproducible and is correlates well with other methods that are based on the use of mucous surfaces [39]. Therefore the method is recommended for the screening analysis of mucoadhesive properties for micro- and nano-particles of a different nature and composition, e.g. made of chitosan [41] or polyelectrolytes [42].

The loading of commercial mucin derived from the pig stomach (in the concentration of 1 mg mL^{-1}) into vaterite microcrystals during the crystal formation (co-precipitation) and via adsorption on preformed crystals has been studied in our previous work [43]. The loading of mucin was higher for the co-precipitation compared to the adsorption. At the same time, the change in the surface charge of the particles for the co-precipitation was found to be less than that for the adsorption method. The co-precipitation of mucin has been recommended for BAS inclusion into the vaterite crystals; this process mainly corresponds to the biomineralization on mucous surfaces [44]. In the past decades, layer-by-layer (LbL) assembly of biomacromolecules of various nature has been shown as versatile tool allowing fine control over the biomaterials' structure for biomedical and biomimetic applications [45–47]. The ability to employ mucin as a polyanion in sequential LbL adsorption of molecules on vaterite microcrystals has been demonstrated that is in a good agreement with results reported on mucin adsorption on

other surfaces [48–50] as well as mucin interactions with water-soluble polymers [51]. However, adsorption of mucin on vaterite microcrystals at concentrations of mucin relevant to actual concentrations in the mucus has not been studied yet. In addition, an effect of adsorption conditions and mucin properties is also not reported.

This work continues our recent study [43] and aims to investigate how does the adsorption of mucin on vaterite microcrystals depend on environmental conditions, i.e. (pH, ionic strength, the presence of organic solvents and detergents), adsorption time and glycoprotein concentration. This will allow to predict the mucoadhesive properties of vaterite microcrystals and crystal behavior in mucosal environment. In addition, herein we continue the development of approaches to stabilize microcrystals loaded with mucin via the LbL deposition of polyelectrolytes which has been reported recently [43] and is highly promising for the development of test systems based on vaterite for studying the mucoadhesiveness of various objects such as polymers, particles and microorganisms.

2. Experimental section

2.1. Materials

Calcium chloride anhydrous, ≥93.0% (C1016), sodium carbonate Na_2CO_3 anhydrous, ≥99.0% (S7795), commercial mucin from porcine stomach, Type III, (m1778), bound sialic acid 0.5–1.5%, protamine from salmon, fluorescein isothiocyanate isomer 1 (FITC), 2,4,6-trinitrobenzenesulfonic acid (TNBS), *N*-acetylneuraminic acid from E. coli, ethylenediaminetetraacetic acid (EDTA), gel filtration molecular weight markers kit MW 12–200 kDa (Sigma-Aldrich); 5,5′-dithiobis(2-nitrobenzoic acid) (DTNB) (Serva, Germany); cysteine, >99.5% (BioUltra); Sephadex G-200 (Pharmacia) were used. All chemicals used for the preparation of buffer solutions were laboratory grade and purchased from Sigma–Aldrich. Before use, mucin solutions were sonicated for 30–90 min using the ultrasonic bath (Elmasonic S15H, Germany).

2.2. Analytical determination of mucin

The concentration of the glycoprotein mucin in solutions was determined spectrophotometrically at the wavelengths of 214 nm and 260 nm [52] or employing analytical size exclusion chromatography using the column Biofox 17 *SEC* 8 × 300 mm (Bio-Works, Sweden) in 0.15 M NaCl (the chromatographic system Smartline (Knauer, Germany) [43]. Preliminary, both methods were calibrated using solutions of purified mucin with different concentrations in the ranges 0.01–0.1 or 0.01–1 mg mL^{-1}. The column was additionally calibrated using model proteins with different molecular weights.

2.3. Purification of mucin via chromatography

15–45 mL of the mucin solution (5 mg mL^{-1}) was subjected to the column filled with Sephadex G-200 (dimension 2.5 × 35 cm) using the chromatographic system Bio-Logic LP (Bio-Rad, USA) in the solution of ammonia (pH 9.0) with the elution rate of 0.5 mL min^{-1} and collection time for one fraction of eluted solution of 12 min. Absorbance was determined in the obtained fractions at the wavelengths of 214, 260, and 480 nm. The fractions containing mucin, as identified by absorbance and specific determination by the Schiff's method, were combined and freeze-dried as described in [43].

2.4. Synthesis of Mucin-FITC

Commercially available mucin (4.5 mg mL^{-1}) has been labelled as described in [43] using 1 mg mL^{-1} FITC (dissolved in dimethylformamide) and carrying out the reaction in 0.5 M carbonate buffer with pH 9.0 for 24 h at 4 °C. The solution was exposed to chromatography analysis and the molar modification degree of the free amino groups in mucin-FITC was found to be 17 ± 2% relative to purified mucin [43].

2.5. Synthesis of desialated mucin

Commercially available mucin (0.3 mg mL^{-1}) has been exposed to the solution of 0.01 M HCl and incubated for 3 h at 80 °C. The solution was exposed to chromatography analysis using the column filled with Sephadex G-200, as described above. The content of sialic acids was found to be 2.30 ± 0.10 and 0.41 ± 0.05% for initial mucin and desialated mucin, respectively, as reported in [43].

2.6. Mucin loading into the $CaCO_3$ crystals by adsorption

The $CaCO_3$ crystals were formed according to the standard procedure [19] by adding of the solution of $CaCl_2$ to the equimolar solution of Na_2CO_3. The crystals were washed twice with water and dried in the oven at 70 °C. The aqueous suspension of $CaCO_3$ crystals (20 mg mL^{-1}) was agitated with 1–6 mg mL^{-1} mucin solution on a shaker for 30 min. The precipitate was separated by centrifugation (2 min, 1000 g) followed by removal of the supernatant and double washing with water. The content of mucin was determined in the supernatant and the washing solutions.

The amount of the loaded protein at equilibrium was calculated using the following equation:

$$q_e = \frac{(c_0 - c_e) \cdot V}{m}$$

where q_e – the adsorption capacity (mg g^{-1}), c_0 and c_e – the initial and equilibrium mucin concentrations, respectively (mg mL^{-1}); V is the volume (mL) of the mucin solution; and m is the mass of $CaCO_3$ (g).

2.7. Kinetics of mucin adsorption

The kinetics of mucin adsorption was monitored with respect to the loss of mucin in solution by absorbance at 260 nm or with respect to the accumulation of fluorescence signal in vaterite microcrystals in the presence of mucin-FITC as analysed by fluorescence microscopy (EVOS FL, Thermo Fisher Scientific, USA).

For the latest case, the kinetics of mucin loading has separately been assessed for microcrystal interior and its surface. The background fluorescence has been subtracted from the mean fluorescence signal. The photo-bleaching effect during the experiment was found to be insignificant (data not shown) and has been neglected. At least 10 vaterite microcrystals have been analysed for each time point to get an average fluorescence signal.

2.8. Mathematical fitting

Experimental points for kinetics of mucin adsorption (up to 6 h of mucin loading) has been fitted with the three models [53] described below:

1. Pore diffusion model (Bangham's equation):

Among a number of diffusional models, Bangham model has been chosen because the porosity seems to be the most apparent property of the vaterite $CaCO_3$ microcrystals. Bangham equation was applied in the following form:

$$\ln q_t = \alpha \ln t + \ln K$$

2. Pseudo-first order model:

Adsorption kinetics that is described by the pseudo-first order reaction model with the rate constant k obeys the following equation:

$$\ln(q_e - q_t) = -kt + \ln q_e$$

3. Pseudo-second order model:

This model is described by the linear equation:

$$\frac{1}{q_t} = \frac{1}{q_e} + \left(\frac{1}{kq_e^2}\right) \cdot \frac{1}{t}$$

Maximum adsorption capacity has been fixed (35 mg g^{-1}) based on the experimental data. The goodness of the fit was assessed based on R-squared coefficient calculated as $1 - \frac{\sum (y_i - f_i)^2}{\sum (y_i - y_{av})^2}$, where f_i is the predicted value from the fit, y_{av} is the mean of the observed data, y_i is the observed data value.

2.9. LbL deposition of mucin

The LbL deposition of either mucin (control experiment) or mucin and protamine (a pair of polymers used) has been performed on the synthetized vaterite $CaCO_3$ crystals. In either case, the polymer concentration was 0.5 mg mL^{-1} and the crystals concentration was 20 mg mL^{-1}. The coated crystals were washed twice with water and their ζ-potential was measured after each adsorption step. The $CaCO_3$ crystals coated with three (mucin-protamine) bilayers were dissolved by dropwise addition of equimolar amount of 0.2 M EDTA (to solubilize all the crystals), and then the formed polyelectrolyte microcapsules were washed three times with water by centrifugation. The content of mucin in the microcapsules was determined by determination of mucin content in washing solutions obtained during the capsule preparation procedure.

2.10. Characterization of the crystals and capsules

Analysis of microparticles prepared in this study ($CaCO_3$ crystals and polyelectrolyte capsules) was carried out using light optical microscopy (Carl Zeiss JENA, Germany) and scanning electron microscopy (SEM, Zeiss DSM 40, Germany). The size of the nanocrystallines (the $CaCO_3$ crystals are made of) was determined from particle surface analysis in SEM photographs, as described in [10]. Determination of hydrodynamic diameter of commercial mucin (0.1 mg mL^{-1}) was carried out using dynamic light scattering (DLS, Malvern Zetasizer Nano ZS, UK). A suspension of microparticles (0.5 mg mL^{-1}), solutions of 0.1 mg mL^{-1} mucin or protamine were used DLS. Electrophoretic mobility of mucin, protamine and vaterite microcrystals (pure or coated with mucin/protamine layers) was measured under the same conditions using Malvern Zetasizer Nano ZS, UK. ζ-potentials have been calculated using the Smoluchowski equation.

3. Results and discussion

3.1. Physical-Chemical properties of vaterite microcrystals coated with mucin

Vaterite microcrystals were obtained by mixing equimolar solutions of $CaCl_2$ and Na_2CO_3 (Fig. 2, No. 1). According to SEM images (Fig. 3a), the dried crystals used in this study had spherical shape with an average diameter of 3.3 ± 0.8 μm. The average diameter of nanocrystallines in the crystal was 109 ± 25 nm that corroborates well with literature data [10]. The pore size in the microcrystals prepared by similar procedure has previously been determined by Brunauer-Emmett-Teller adsorption/desorption method and was found to be in the range 5–40 nm [19]. The surface charge of the crystals dispersed in water appeared to be 9 ± 1 mV as measured by DLS.

The commercial mucin from the pig's stomach (further - mucin) was used in this study. Mucin had a surface charge of −15 ± 2 mV according to DLS in the solution of 1 mg mL^{-1} (Fig. S1) and was represented by two fractions with hydrodynamic diameters in the range 30–50 and 200–300 nm, respectively (Fig. S2). Purified, FITC-labelled and desialated mucins were prepared from commercial mucin and gel filtrated. These mucins contained only a short fraction with a hydrodynamic diameter in the range 30–50 nm because the heavy fraction has been filtered off.

SEM imaging of the microcrystals loaded with mucin did not reveal any significant changes in the morphology of the vaterite crystals (Fig. 3b): microsphere diameter 3.6 ± 1.1 μm, nanocrystallite size 80 ± 18 nm. According to results of the light microscopy analysis, mucin-coated vaterite microcrystals have been found to be present in less aggregated state in water suspension. In addition, they are significantly less prone to recrystallization into more stable calcite polymorph during storage in water compared to uncoated vaterite microcrystals. According to the DLS results, the adsorption of mucin on vaterite microcrystals resulted in a slight change of zeta-potential to the negative value of −15 ± 3 mV, which indicates the binding of mucin to the crystal surface. This is in a good agreement with the results presented in our previous work [43] that compares two methods of mucin adsorption into vaterite crystal: pre-loading (conventionally called co-synthesis) and post-loading (adsorption) of mucin. Herein, we focused on mucin post-loading (Fig. 2, No. II) that has been studied under the constant concentration (20 mg mL^{-1}) of vaterite microcrystals, while the loading time, medium and mucin concentration (II-a) as well as a number of deposition steps for mucin multiple adsorption (II-b) have been varied.

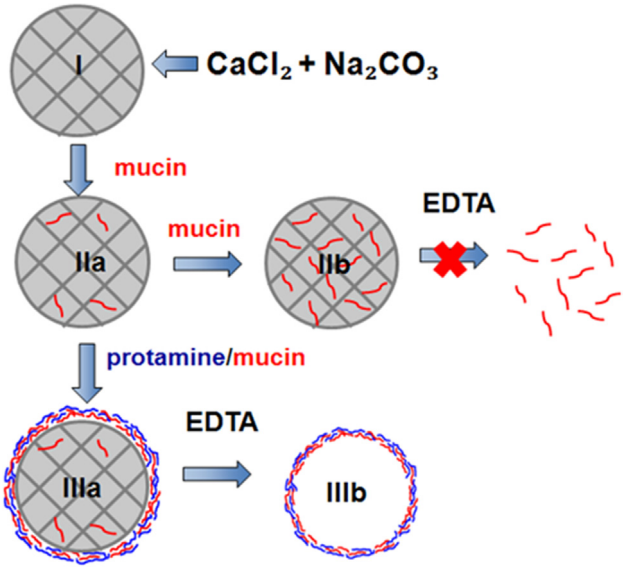

Fig. 2. The scheme of the preparation of mucin-containing microparticles: I – vaterite microcrystals; IIa and IIb – microcrystals coated with one and multiple mucin layers, respectively; IIIa – microcrystals sequentially coated with oppositely charged layers of protamine and mucin; IIIb – $(PRO/MUC)_3$ microcapsules obtained after elimination of $CaCO_3$ from the coated crystals using EDTA. . Adopted from [43]

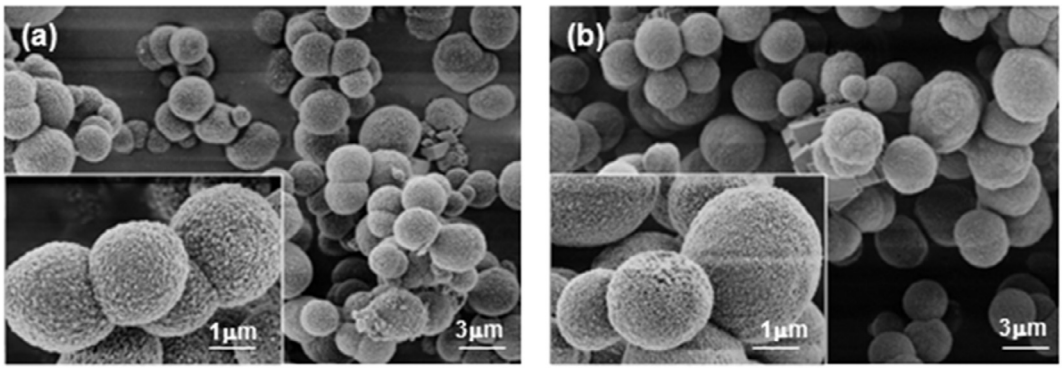

Fig. 3. SEM images of vaterite microcrystals before (a) and after (b) mucin adsorption.

3.2. Kinetics of mucin adsorption

Kinetical analysis of mucin adsorption (Fig. 4) has revealed that the amount of mucin adsorbed on the vaterite microcrystals sharply increased in the first 10 min followed by the gradual down for the next 5 h and then consequently reached the plateau.

The process of adsorption into porous matrices is usually considered as three sequential steps of (i) mass transfer from the bulk to the solid surface followed by (ii) surface adsorption and (iii) diffusion of the adsorbate into the adsorbent interior. Typically, diffusion in the bulk is not considered as a rate-limiting step because of typically applied elimination of diffusional limitations by mechanical stirring of the solution. Some models of adsorption kinetics assume that the sorption is the rate-limiting step, while for other models it is supposed that the diffusion is the rate-limiting step. Mathematical fitting to the models allows the prediction of the adsorption mechanism.

In this study, we applied three well-known models, namely pore diffusional model proposed by Bangham and two commonly used adsorption models of pseudo-first (PFO) and pseudo-second order (PSO) (Fig. 4 and Table S1) [53]. All of them are applicable for homogeneous adsorption of mucin on spherical particles from solutions with the concentration of mucin far away from saturation (below mucin solubility). The best fitting to the Banham model (R^2 0.999 vs. 0.769 and 0.106 for PSO and PFO, respectively) indicates that the diffusion of mucin inside vaterite $CaCO_3$ microcrystals through the pores is the slowest and thus the rate-limiting step in mucin adsorption.

In order to put more evidence on adsorption mechanism and understand the distribution of glycoprotein in vaterite microcrystals, the kinetics of adsorption of mucin-FITC was also studied by means of fluorescence microscopy (Fig. 5). Immediately after exposure of vaterite crystals into mucin-FITC solution, the glycoprotein was mainly located on the surface of the crystals (Fig. 5a–c). This was followed by further accumulation of more mucin-FITC on the crystal surface and partial permeation of mucin-FITC inside the microcrystals during the next 30 min of incubation (Fig. 5d–f). The kinetics of accumulation of fluorescence signal on the crystal surface and inside the crystals has been investigated (Fig. 5g) showing that the adsorption on the surface of the crystals occurs faster compared to the accumulation of mucin-FITC in the crystal interior.

Altogether, these results allow to propose that the rate of mucin adsorption is determined by diffusion of mucin into the pores of the vaterite microcrystals rather than its adsorption on the crystal surface.

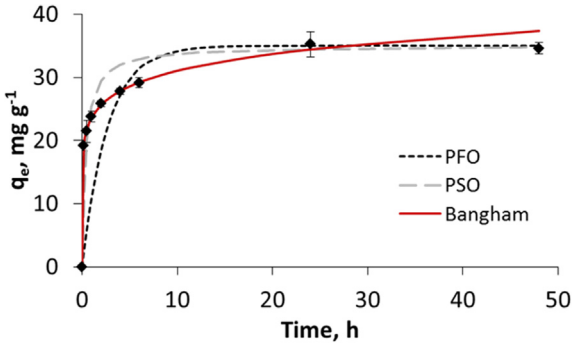

Fig. 4. Kinetics of mucin adsorption on vaterite microcrystals (initial concentration of mucin is 1 mg mL^{-1}). Cumulative amount of mucin adsorbed on $CaCO_3$ crystals (q_e) was determined by the absorbance at 260 nm. Black rhombs – experimental points, mathematical fitting with three models is shown by solid and interrupted lines.

3.3. Influence of mucin concentration on adsorption capacity of the microcrystals

It is known that mucin concentration determines its aggregation and gelling properties [33]. This motivated us to investigate the influence of the concentration of commercial mucin in the range of 1–6 mg mL^{-1} on its adsorption to the vaterite microcrystals (Fig. 6a). The upper value of the tested concentration of mucin was chosen to be similar to the concentration of mucin in the mucus of the gastrointestinal tract [34]. Based on these data, an isotherm of mucin adsorption was constructed (Fig. 6b) and analyzed on the basis of the assumptions of Langmuir monolayer adsorption according to the classical equation below:

$$q_e = \frac{q_{max} K_a c_e}{1 + K_a c_e}$$

where q_e – equilibrium adsorption capacity (mg g^{-1}); c_e – concentration of mucin in the solution at equilibrium (mg mL^{-1}); q_{max} – maximum adsorption capacity (mg g^{-1}); K_a – adsorption equilibrium constant (mL mg^{-1}).

Adsorption isotherm was further plotted in linear coordinates $1/q_e = f(1/c_e)$. Maximum adsorption capacity q_{max} of 159 ± 9 mg g^{-1} and the adsorption equilibrium constant K_a = 2.52 mL mg^{-1} were calculated with the coefficient of determination R^2 of 0.994. The q_{max} obtained is 4.6 times higher and the K_a is 3.6 times lower than those values determined for adsorption of high-molecular-weight enzyme catalase (250 kDa, pI 5.4) to the crystals. The enzyme has a similar sign of a charge under the adsorption conditions but a smaller diameter of 10 nm [11].

In addition, the Gibbs free energy of the adsorption process was calculated as follows:

$$\Delta G = -RT \cdot lnK_a$$

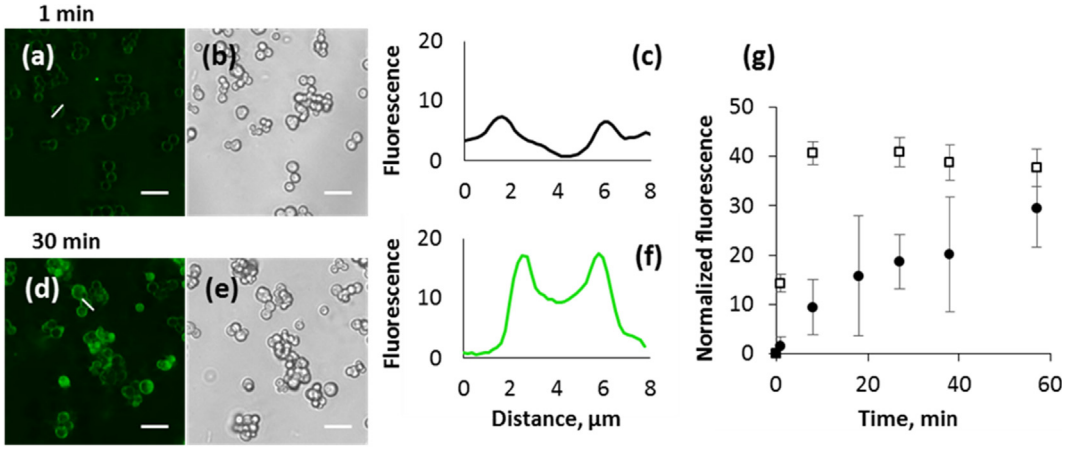

Fig. 5. Fluorescence (a,d) and optical transmittance (b,e) images of $CaCO_3$ crystals after 1 and 30 min of incubation in mucin-FITC solution, respectively. Fluorescent profiles (c,f) are taken along the white lines in the images (a) and (d) showing the distribution of mucin-FITC inside $CaCO_3$ crystals after 1 and 30 min incubation, respectively. Scale bars are 10 μm. (g) kinetics of mucin-FITC adsorption on the surface of $CaCO_3$ microcrystals (white squares) and kinetics of penetration of mucin-FITC inside vaterite crystals (black circles).

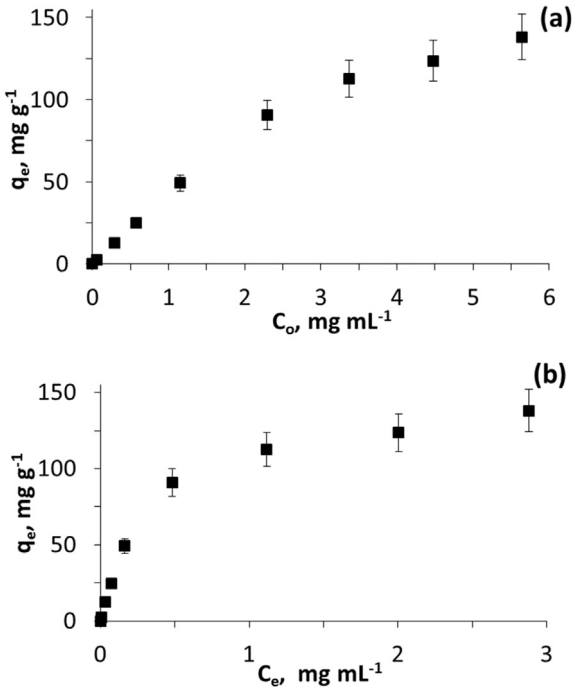

Fig. 6. Mucin adsorption capacity on vaterite microcrystals as a function of initial (a) and equilibrium (b) concentration of the glycoprotein. q_e was determined after 30 min of incubation by measurements of the absorbance at 260 nm.

where R is the universal gas constant, 8.31 (J K^{-1} mol^{-1}); T is the temperature (K); K_a is the constant of adsorption equilibrium (L mol^{-1}).

The Gibbs energy of the mucin adsorption process was found to be -35 ± 4 kJ mol^{-1} and was in a good agreement with the value for catalase and a number of other previously studied proteins [11]. Negative value of Gibbs free energy for mucin adsorption indicates a significant shift in the equilibrium towards adsorption. This in turn gives a high content of mucin in the crystals: at a maximum adsorption capacity, mucin content can reach a value of up to 16% by the mass of the vaterite crystals.

Interestingly, some less abundant mucus proteins (e.g., lysozyme) have lower adsorption capacity for vaterite crystals compared with mucin (about 15 mg g^{-1} for lysozyme post-loading in $CaCO_3$ [54]). The same is also valid for serum albumin (ca 20 mg g^{-1}) [54]. This extremely high affinity of $CaCO_3$ crystals to mucin might open prospects for the use of vaterite crystals for selective mucosal delivery in future.

3.4. The role of mucin purification and desialization

In addition, the adsorption capacities of commercial, purified and desialated mucins (prepared by analytical chromatography) on vaterite microcrystals were studied and compared. Purified mucin has the largest negative surface charge of -27 ± 1 mV and its adsorbed mass on microcrystals was by 25 ± 3% more than that for commercial mucin. This can be explained by higher capacity of the crystals for smaller mucin molecules as they can permeate into the pores of the crystals where more surface is available for adsorption. The desialated mucin (degree of desialization 80%) was adsorbed on microcrystals giving by 1.5 times less adsorbed amount than that for commercial mucin. The difference in the adsorption of mucin preparations evidences an important role of sialic acids and, consequently, a role of electrostatic interactions during the adsorption of the glycoprotein. Consequently, an increase in the content of sialic acids in mucin can lead to strengthening the binding of mucin by microcrystals. We believe this is an important finding for future study on mucin adsorption, as in the case of cancer diseases, the content of sialic acids in mucins increases [55]. Taking into account that $CaCO_3$ crystals have been recently proposed as anticancer delivery carriers [5,56], the elevated levels of sialic acid in mucosal cancer might enhance the uptake of vaterite-based delivery systems by the mucus surrounding cancer cells.

3.5. The influence of adsorption medium

The charge, conformational and aggregative states as well as rheological properties of mucin significantly depend on its environmental conditions [57–60]. This stimulated us to investigate the adsorption of mucin on vaterite microcrystals exposed into medium with different pH ($5 \cdot 10^{-3}$ M TRIS buffer solution, pH 7–9), ionic strength (the presence of 0.15–1.0 M NaCl at pH 7.1) and in the presence of organic solvent (20% isopropanol) of surfactant (0.0035 M SDS). The cumulative amount of bound mucin has been compared with the control value for glycoprotein adsorption from water solution (Fig. 7). One can expect a contribution of elec-

trostatic and hydrophobic interactions to the binding of mucin to the crystals. Below the experimental results are discussed in a view of the expected interactions.

The amount of mucin adsorbed to the microcrystals slightly increased with increasing pH from 7 to 9. This can be explained by the stable negative charge of mucin in the studied pH range that is much above the pI of mucin, i.e. 3–4 [33] and rather low charge of the vaterite microspheres [4]. Thus, variation of pH in this range does not significantly affect the adsorption process as variations of electrostatic interactions are not expected. The addition of NaCl up to physiological values (0.15 M) resulted in the slight increase of adsorption capacity. This phenomenon can be explained by a decrease in the electrostatic repulsion between the glycoprotein molecules in the presence of salt (charge screening), which agrees well with the results of [57]. Reduced repulsive interactions between mucin molecules can allow more mucin molecules to be loaded into the pores of the crystals. Herein, it seems that at low NaCl concentrations the strengthening of mucin-mucin interaction dominates over the diminution of mucin-$CaCO_3$ attraction. With further increase of the salt concentration up to 1 M, the amount of bound mucin gradually decreases that may be due to significant screening of charges at high salt concentration that can weaken on electrostatic attraction of mucin to $CaCO_3$ resulting in less amount of the adsorbed mucin. In this way, the abolishment of mucin-$CaCO_3$ attraction dominates over increasing intermolecular mucin interactions. At the same time substantial amount of adsorbed mucin even at very high ionic strength (1 M NaCl) points on the presence of non-Coulombic interactions between mucin and the crystals and/or intermolecular mucin interactions. This can most probably be attributed to hydrophobic interactions that can take place between mucin molecules.

The presence of 20% isopropanol did not alter the amount of mucin adsorbed as compared with the adsorption from aqueous medium, which also supports a significant or even a dominating contribution of hydrophobic interactions into the mucin binding to the crystals. Otherwise an effect of solvent polarity should be pronounced.

The presence of 0.0035 M sodium dodecyl sulfate results in significant drop (ca 57%) in the amount of adsorbed mucin. One can explain this by removal of mucin molecules from pores of the crystals due to strong binding to SDS and mucin in solution as driven by hydrophobic interactions. This assumption is in a line with the crucial role of hydrophobic interactions as described above.

Concluding from the above, the adsorption of mucin, and, consequently, the mucoadhesive properties of the vaterite microcrystals, can considerable be varied depending on the environmental conditions.

3.6. Stepwise mucin adsorption

The effect of stepwise LbL adsorption of mucin on the vaterite microcrystals (Fig. 2-IIb) was considered. This differs from our previous studies [43], where the mucin was loaded into the crystals by co-precipitation. At each of the six adsorption steps, vaterite microcrystals (20 mg mL^{-1}) were consequently incubated in 0.5 mg mL^{-1} mucin solution, centrifuged and washed with water (Fig. 8). An increase in the number of adsorption steps is accompanied by a decrease in the stepwise binding of mucin and simultaneous increase in the total adsorption of mucin by the crystals. At the same time, an increase in the number of adsorption steps did not cause the changes in the charge of microcrystals, which varied in the range from −12 to −15 mV. This phenomenon can occur due to redistribution of mucin on the surface of crystals or possible additional binding between the layers of mucin due to the formation of intermolecular disulfide, hydrogen bonds and hydrophobic interactions. Our further studies using Elman's method [61] helped to reveal the absence of free SH groups in mucin meaning that the formation of additional disulfide bonds should not occur. Thus, hydrogen bonding and hydrophobic interactions between mucin molecules seem to play a vital role in adsorption of mucin resulting in formation of multiple mucin layers. Similar explanation has been proposed for the stepwise adsorption of mucin on vaterite crystals pre-loaded with mucin [43].

The microcrystals coated with six layers of mucin (Fig. S3) were treated with EDTA to dissolve solid $CaCO_3$ that led to spontaneous disintegration of the particles (Fig. 2, No. II). The same behavior has been reported for twice less number of adsorbed layers [43] which indicates that mucin multilayers cannot be stabilized solely by hydrogen bonding and hydrophobic interactions. Such a low performance of mucin retention into vaterite microcrystals can be improved by employing the LbL adsorption of the glycoprotein in a pair with a polycation. These results are shown and discussed below.

3.7. The LbL mucin/protamine adsorption on vaterite microcrystals

The retention of adsorbed mucin on vaterite microcrystals for the LbL deposition of mucin and an oppositely charged polycation (Fig. 3,

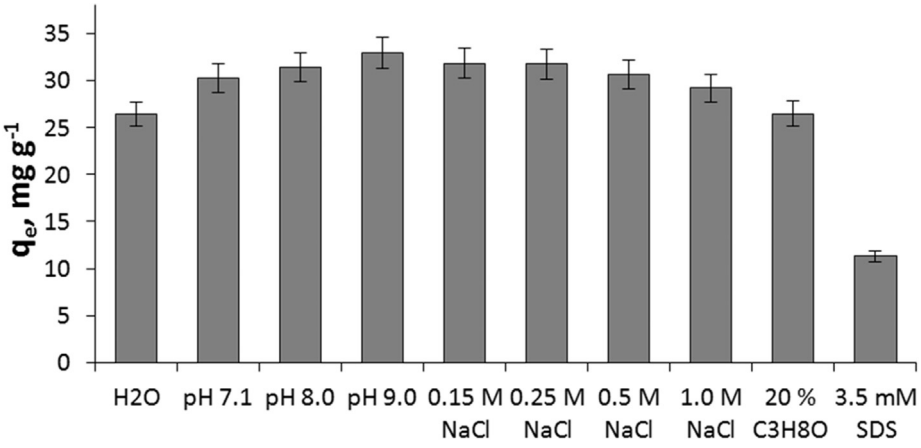

Fig. 7. The influence of the composition of the medium on the equilibrium adsorption capacity (q_e) of vateriate crystals for commercial mucin (mg g^{-1}) on vaterite microcrystals. Adsorption capacities are determined by absorbance at 260 nm after the incubation in the medium (5 mM TRIS buffer) during 1 h. Initial concentration of mucin is 1 mg mL^{-1}, 20 mg mL^{-1} of vaterite crystals are used in all the experiments.

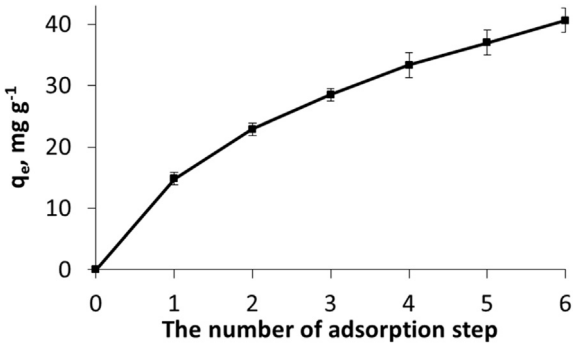

Fig. 8. Stepwise multiple mucin adsorption on vaterite microcrystals. Adsorption capacities are determined by the measuring an absorbance of supernatants at 260 nm.

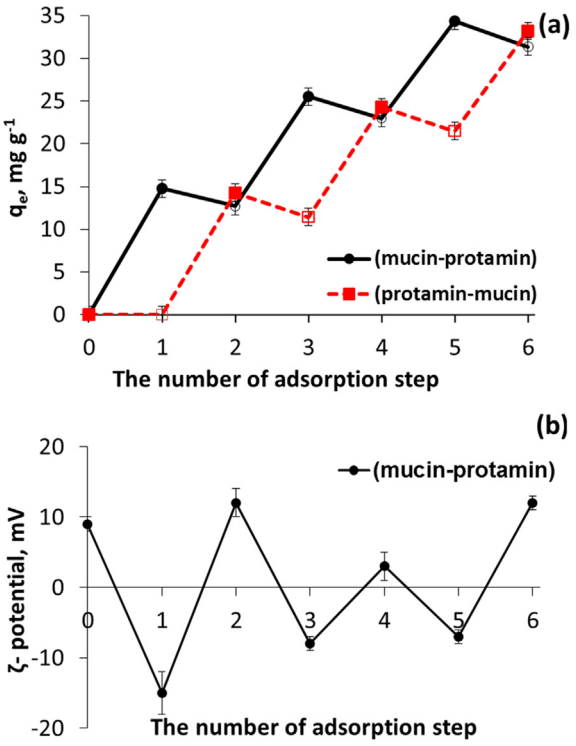

Fig. 9. (a) The amount of mucin adsorbed on vaterite microcrystals during sequential deposition of $(mucin/protamine)_3$ and $(protamine/mucin)_3$ coatings. The steps of mucin adsorption are shown with filled markers; adsorption of protamine corresponds to non-filled markers. Adsorption capacities are determined by measuring mucin absorbance in supernatants at 260 nm. (b) The change of zeta-potential of the microcrystals during sequential deposition of $(mucin/protamine)_3$ coating. Initial concentrations of mucin and protamine are 0.5 and 1.0 mg mL^{-1} for each deposition step, respectively.

No. IIIb) was investigated. For this, polypeptide protamine (5 kDa, pI 11, zeta potential in water solution + 7 mV) that is actively used as a model biologically relevant polyelectrolyte [62] has been chosen.

In continuation of our recent study [43] where the stability of $(mucin\text{-}protamine)_3$ capsules have been proven by optical microscopy, the LbL adsorption of protamine and mucin was investigated for either protamine or mucin used as a first deposition layer (Fig. 9). After each adsorption step, the microcrystals were washed twice to remove unbound polyelectrolyte. Fig. 9a shows the dependence of the amount of mucin loaded into microcrystals from a deposition step, which was determined by measuring the glycoprotein concentration in the supernatant and washing solutions and is referred to the mass of the initial $CaCO_3$. The amount of bound mucin increased during the adsorption of mucin and slightly decreased during the following adsorption of protamine, indicating replacement of some amount of mucin during deposition of the polycation. This is in a good agreement with the data obtained for LbL deposition of mucin with other polycations such as polyallylamine hydrochloride [63], chitosan [64] and lactoperoxidase [48,65].

Interestingly, as can be concluded from the Fig. 9a, the amount of bound mucin almost did not depend on the sequence of the polyelectrolyte deposition steps (defined by the first layer). This phenomenon can be explained by low adsorption of protamine onto vaterite microcrystals as a first layer, which was demonstrated earlier in our work in which the polypeptide was almost completely eluted from crystals during washing (q_m 2.6 ± 0.1 mg g^{-1}) [11]. At the same time the observed phenomenon can be explained by a significant role of intermolecular interactions between mucin molecules as discussed above. This would reduce an impact of electrostatic interactions to complexation of mucin and protamine. Both factors described above may be responsible for no effect of a sequence of polymers deposited on the absolute amount of adsorbed mucin as a function of a number of layers.

The adsorption of polyelectrolytes led to the recharging of the surface of microcrystals from negative values for mucin deposition steps to positive values for protamine deposition, which confirms the formation of a polyelectrolyte complex between mucin and protamine (Fig. 9b) and indicate electrostatic attraction between polymers. However, the values of zeta-potential are rather low (absolute values do not exceed 15 mV) indicating low charge density on the surface of the polymer-coated crystals.

Vaterite microcrystals coated with three polyelectrolyte bilayers, regardless of the polyelectrolyte application sequence used, were stable during storage in water at 4 °C without recrystallization into calcite for 3 months. This shows a strong stabilization effect. Typically bare crystals are recrystallized in water upon overnight storage. More stable non-porous calcite polymorph is formed from less thermodynamically stable vaterite. Here the coating stops the recrystallization most probably by suppression of ion diffusion from the crystal surface since this solution-mediated process is supposed to be responsible for the recrystallization. Such strong stabilization can be utilized in future for preparation of mucoadhesive carriers with long term BAS delivery options.

The dissolution of $(mucin/protamine)_3$ coated $CaCO_3$ crystals with 0.2 M solution of EDTA resulted in the formation of polymer microcapsules (Fig. 2, IIIb). This confirms the stabilization of polyelectrolyte layers by electrostatic interactions, because the crystals coated with only mucin layers completely dissolved in the presence of EDTA. Most probably the hydrophobic interactions between mucin molecules are strong but their strength is not enough to keep one-component mucin capsules intact. High flux of ions during the crystal dissolution may affect stability of polymer coating and stable coating can resist the high osmotic shock only if multiple cooperative interactions (both electrostatics and hydrophobic interaction) are involved. It should be noted that simplistic hollow structure of the capsules shown in Fig. 2 (IIIb) can differ from actual structure of the capsules that might appear as matrix-type capsules due to possible presence of mucin inside the capsule lumen. Internal structure of the capsules requires further clarification.

4. Conclusion

The adsorption of mucin on mesoporous vaterite microcrystals has been investigated. The loading of mucin does not affect the structure of vaterite crystals. The study of adsorption kinetics demonstrated a rapid loading of mucin at initial time of adsorption followed by slow adsorption step for ca 5 h. Bangham adsorption

model described the kinetics much better than pseudo-first and pseudo-second order models. This adsorption kinetics has been explained from the view of pore diffusional model meaning that the diffusion of mucin inside vaterite crystals is supposed to be a rate-determine step. This conclusion was also supported by direct observation by fluorescence microscopy focusing on mucin localization into the crystals.

Analysis of mucin adsorption at varied pH, ionic strength, and polarity of a solvent allow to suggest a contribution of both electrostatics and hydrophobic interaction into the mucin-crystal binding. This is also supported by observation of layer-by-layer deposition of mucin and protamine onto the crystals as well as stability observations for multilayer one-component mucin/mucin and two-component mucin/protamine capsules. There is no effect of a deposition sequence for the layer-by-layer deposition of mucin and protamine that may be due to significant impact of intermolecular mucin-mucin hydrophobic interactions. However, despite this, pure mucin/mucin capsules are not stable compared to well-defined mucin/protamine ones indicating an impact of electrostatics. Electrostatic interactions are also revealed by zeta-potential measurements for mucin/protamine coating and by study on adsorption of desialated mucin onto the crystals. Mucin adsorption studied here is characterized by thermodynamic parameters such as the Gibbs free energy (-35 ± 4 kJ mol^{-1}) and equilibrium constant (K_a = 2.52 - mL mg^{-1}). Those parameters are well in a line with results obtained for adsorption of a number of model proteins indicating similar behavior of the glycoprotein mucin compared to pure proteins.

The results obtained on the influence of environmental conditions on mucin adsorption lead to the conclusion that vaterite microcrystals can adsorb substantial amount of mucin (ca. 16% by mass), and, consequently, bind to mucus, i.e. possess mucoadhesive properties. It is possible to make an assumption about the retention of microcrystals by a mucus surface and the prospects for their use for mucosal drug delivery. High adsorption of mucin on vaterite microcrystals seems to be promising finding for the use of this glycoprotein as a polyanion for layer-by-layer polyelectrolyte adsorption and, subsequently, preparation of polyelectrolyte microcapsules. Stabilization of vaterite crystals by mucin adsorption and the production of mucin-containing microcapsules is considered as an interesting and promising approach for the development of the test-systems for the purpose of studying the mucoadhesive properties of various objects, for example, polymers [66], nanoparticles [40,67] and microorganisms [68].

Conflict of interest

The authors declare no conflict of interest.

Acknowledgements

This work was carried out with the financial support of M.V. Lomonosov Moscow State University (topic AAAA-A16-116052010081-5). This work was supported in part by M.V. Lomonosov Moscow State University Program of Development. A.V. acknowledges QR Fund from Nottingham Trent University and thanks the Europeans Union's Horizon 2020 research and innovation programme for funding (the Marie-Curie Individual Fellowship LIGHTOPLEX-747245).

Appendix A. Supplementary material

Supplementary data to this article can be found online at https://doi.org/10.1016/j.jcis.2019.03.042.

CRediT authorship contribution statement

Nadezhda G. Balabushevich: Conceptualization, Investigation, Methodology, Project administration, Resources, Supervision, Validation, Writing - original draft, Writing - review & editing. **Ekaterina A. Kovalenko:** Formal analysis, Investigation, Methodology. **Elena V. Mikhalchik:** Formal analysis, Investigation, Methodology, Supervision, Validation, Writing - review & editing. **Lyubov Y. Filatova:** Formal analysis, Investigation, Methodology, Supervision, Validation, Writing - review & editing. **Dmitry Volodkin:** Conceptualization, Data curation, Funding acquisition, Project administration, Resources, Software, Supervision, Validation, Writing - original draft, Writing - review & editing. **Anna S. Vikulina:** Conceptualization, Data curation, Funding acquisition, Project administration, Resources, Software, Supervision, Validation, Writing - original draft, Writing - review & editing.

References

[1] D.V. Volodkin, A.I. Petrov, M. Prevot, G.B. Sukhorukov, Matrix polyelectrolyte microcapsules: new system for macromolecule encapsulation, Langmuir 20 (2004) 3398–3406.
[2] N.G. Balabushevich, V.A. Izumrudov, N.I. Larionova, Protein microparticles with controlled stability prepared via layer-by-layer adsorption of biopolyelectrolytes, Polym. Sci. Ser. A 54 (2012) 540–551.
[3] Y.-H. Won, H.S. Jang, D.-W. Chung, L.A. Stanciu, Multifunctional calcium carbonate microparticles: synthesis and biological applications, J. Mater. Chem. 20 (2010) 7728.
[4] D. Volodkin, $CaCO_3$ templated micro-beads and -capsules for bioapplications, Adv. Colloid Interface Sci. 207 (2014) 306–324.
[5] S. Maleki Dizaj, M. Barzegar-Jalali, M.H. Zarrintan, K. Adibkia, F. Lotfipour, Calcium carbonate nanoparticles as cancer drug delivery system, Exp. Opin. Drug Deliv. 12 (2015) 1649–1660.
[6] S. Biradar, P. Ravichandran, R. Gopikrishnan, V. Goornavar, J.C. Hall, V. Ramesh, S. Baluchamy, R.B. Jeffers, G.T. Ramesh, Calcium carbonate nanoparticles: synthesis, characterization and biocompatibility, J. Nanosci. Nanotech. 11 (2011) 6868–6874.
[7] E.A. Genina, Y.I. Svenskaya, I.Y. Yanina, L.E. Dolotov, N.A. Navolokin, A.N. Bashkatov, G.S. Terentyuk, A.B. Bucharskaya, G.N. Maslyakova, D.A. Gorin, V.V. Tuchin, G.B. Sukhorukov, In vivo optical monitoring of transcutaneous delivery of calcium carbonate microcontainers, Biomed. Opt. Exp. 7 (2016) 2082–2087.
[8] R. Roth, J. Schoelkopf, J. Huwyler, M. Puchkov, Functionalized calcium carbonate microparticles for the delivery of proteins, Eur. J. Pharm. Biopharm. 122 (2018) 96–103.
[9] M.S. Savelyeva, A.A. Abalymov, G.P. Lyubun, I.V. Vidyasheva, A.M. Yashchenok, T.E.L. Douglas, D.A. Gorin, B.V. Parakhonskiy, Vaterite coatings on electrospun polymeric fibers for biomedical applications, J. Biomed. Mater. Res. A 105 (2017) 94–103.
[10] N. Feoktistova, J. Rose, V.Z. Prokopović, A.S. Vikulina, A. Skirtach, D. Volodkin, Controlling the vaterite $CaCO_3$ crystal pores. Design of Tailor-Made Polymer Based Microcapsules by Hard Templating, Langmuir 32 (2016) 4229–4238.
[11] N.G. Balabushevich, A.V. Lopez de Guerenu, N.A. Feoktistova, D. Volodkin, Protein loading into porous $CaCO_3$ microspheres: adsorption equilibrium and bioactivity retention, Phys. Chem. Chem. Phys. 17 (2015) 2523–2530.
[12] K. Sato, M. Seno, J.-I. Anzai, Release of insulin from calcium carbonate microspheres with and without layer-by-layer thin coatings, Polymers 6 (2014) 2157–2165.
[13] L.N. Hassani, F. Hindré, T. Beuvier, B. Calvignac, N. Lautram, A. Gibaud, F. Boury, Lysozyme encapsulation into nanostructured $CaCO_3$ microparticles using a supercritical CO_2 process and comparison with the normal route, J. Mater. Chem. B 1 (2013) 4011.
[14] T.V. Bukreeva, I.V. Marchenko, T.N. Borodina, I.V. Degtev, S.L. Sitnikov, Y.V. Moiseeva, N.V. Gulyaeva, M.V. Kovalchuk, Calcium carbonate and titanium dioxide particles as a basis for container fabrication for brain delivery of compounds, Dokl. Phys. Chem. 440 (2011) 165–167.
[15] N. Qiu, H. Yin, B. Ji, N. Klauke, A. Glidle, Y. Zhang, H. Song, L. Cai, L. Ma, G. Wang, L. Chen, W. Wang, Calcium carbonate microspheres as carriers for the anticancer drug camptothecin, Mater. Sci. Eng. C 32 (2012) 2634–2640.
[16] S. Chen, D. Zhao, F. Li, R.-X. Zhuo, S.-X. Cheng, Co-delivery of genes and drugs with nanostructured calcium carbonate for cancer therapy, RSC Adv. 2 (2012) 1820.
[17] C.-Q. Wang, M.-Q. Gong, J.-L. Wu, R.-X. Zhuo, S.-X. Cheng, Dual-functionalized calcium carbonate based gene delivery system for efficient gene delivery, RSC Adv. 4 (2014) 38623–38629.
[18] H. Shi, L. Li, L. Zhang, T. Wang, C. Wang, D. Zhu, Z. Su, Designed preparation of polyacrylic acid/calcium carbonate nanoparticles with high doxorubicin payload for liver cancer chemotherapy, CrystEngComm 17 (2015) 4768–4773.
[19] A.S. Vikulina, N.A. Feoktistova, N.G. Balabushevich, A.G. Skirtach, D. Volodkin, The mechanism of catalase loading into porous vaterite $CaCO_3$ crystals by co-synthesis, Phys. Chem. Chem. Phys. 20 (2018) 8822–8831.

[20] T.N. Borodina, D.B. Trushina, I.V. Marchenko, T.V. Bukreeva, Calcium carbonate-based mucoadhesive microcontainers for intranasal delivery of drugs bypassing the blood-brain barrier, BioNanoSci. 6 (2016) 261–268.
[21] O. Gusliakova, E.N. Atochina-Vasserman, O. Sindeeva, S. Sindeev, S. Pinyaev, N. Pyataev, V. Revin, G.B. Sukhorukov, D. Gorin, A.J. Gow, Use of submicron vaterite particles serves as an effective delivery vehicle to the respiratory portion of the lung, Front. Pharmacol. 9 (2018) 559.
[22] Y. Jin, R. Yendluri, B. Chen, J. Wang, Y. Lvov, Composite microparticles of halloysite clay nanotubes bound by calcium carbonate, J. Colloid Interface Sci. 466 (2016) 254–260.
[23] M.A. Hood, K. Landfester, R. Muñoz-Espí, Chitosan nanoparticles affect polymorph selection in crystallization of calcium carbonate, Colloids Surf. A 540 (2018) 48–52.
[24] B.V. Parakhonskiy, A. Haase, R. Antolini, Sub-micrometer vaterite containers: synthesis, substance loading, and release, Angew. Chem. Int. Ed. 51 (2012) 1195–1197.
[25] K. Gopal, Z. Lu, M.M. de Villiers, Y. Lvov, Composite phospholipid-calcium carbonate microparticles: influence of anionic phospholipids on the crystallization of calcium carbonate, J. Phys. Chem. B 110 (2006) 2471–2474.
[26] N. Sudareva, O. Suvorova, N. Saprykina, A. Vilesov, P. Bel'tyukov, S. Petunov, Alginate-containing systems for oral delivery of superoxide dismutase. Comparison of various configurations and their properties, J. Microencapsul. (2016) 1–10.
[27] J. Hombach, A. Bernkop-Schnürch, Mucoadhesive drug delivery systems, Handb. Exp. Pharmacol. 251–266 (2010).
[28] R. Shaikh, T.R. Raj Singh, M.J. Garland, A.D. Woolfson, R.F. Donnelly, Mucoadhesive drug delivery systems, J. Pharm. Bioallied Sci. 3 (2011) 89–100.
[29] N. Salamat-Miller, M. Chittchang, T.P. Johnston, The use of mucoadhesive polymers in buccal drug delivery, Adv. Drug Deliv. Rev. 57 (2005) 1666–1691.
[30] C. Valenta, The use of mucoadhesive polymers in vaginal delivery, Adv. Drug Deliv. Rev. 57 (2005) 1692–1712.
[31] M.I. Ugwoke, R.U. Agu, N. Verbeke, R. Kinget, Nasal mucoadhesive drug delivery: background, applications, trends and future perspectives, Adv. Drug Deliv. Rev. 57 (2005) 1640–1665.
[32] A. Ludwig, The use of mucoadhesive polymers in ocular drug delivery, Adv. Drug Deliv. Rev. 57 (2005) 1595–1639.
[33] R. Bansil, B.S. Turner, Mucin structure, aggregation, physiological functions and biomedical applications, Curr. Opin. Colloid Interface Sci. 11 (2006) 164–170.
[34] R. Bansil, B.S. Turner, The biology of mucus: composition, synthesis and organization, Adv. Drug Deliv. Rev. 124 (2018) 3–15.
[35] J. Leal, H.D.C. Smyth, D. Ghosh, Physicochemical properties of mucus and their impact on transmucosal drug delivery, Int. J. Pharm. (Amsterdam, Neth.) 532 (2017) 555–572.
[36] J. Dekker, J.W. Rossen, H.A. Büller, A.W. Einerhand, The MUC family: an obituary, Trends Biochem. Sci. 27 (2002) 126–131.
[37] J.D. Smart, The basics and underlying mechanisms of mucoadhesion, Adv. Drug Deliv. Rev. 57 (2005) 1556–1568.
[38] T. Yu, G.P. Andrews, D.S. Jones, Mucoadhesion and characterization of mucoadhesive properties, in: J. das Neves, B. Sarmento (Eds.), Mucosal Delivery of Biopharmaceuticals, Springer US, Boston, MA, 2014, pp. 35–58.
[39] P. He, S.S. Davis, L. Illum, In vitro evaluation of the mucoadhesive properties of chitosan microspheres, Int. J. Pharm. (Amsterdam, Neth.) 166 (1998) 75–88.
[40] P. Georgiades, P.D.A. Pudney, D.J. Thornton, T.A. Waigh, Particle tracking microrheology of purified gastrointestinal mucins, Biopolymers 101 (2014) 366–377.
[41] D.-W. Lee, S.A. Shirley, R.F. Lockey, S.S. Mohapatra, Thiolated chitosan nanoparticles enhance anti-inflammatory effects of intranasally delivered theophylline, Respir. Res. 7 (2006) 112.
[42] N.G. Balabushevich, M.A. Pechenkin, I.N. Zorov, E.D. Shibanova, N.I. Larionova, Mucoadhesive polyelectrolyte microparticles containing recombinant human insulin and its analogs aspart and lispro, Biochem. Moscow 76 (2011) 327–331.
[43] N. Balabushevich, E. Sholina, E. Mikhalchik, L. Filatova, A. Vikulina, D. Volodkin, Self-assembled mucin-containing microcarriers via hard templating on $CaCO_3$ crystals, Micromachines 9 (2018) 307.
[44] B.D.E. Raynal, T.E. Hardingham, J.K. Sheehan, D.J. Thornton, Calcium-dependent protein interactions in MUC5B provide reversible cross-links in salivary mucus, J. Biol. Chem. 278 (2003) 28703–28710.
[45] V.Z. Prokopovic, A.S. Vikulina, D. Sustr, E.M. Shchukina, D.G. Shchukin, D.V. Volodkin, Binding mechanism of the model charged dye carboxyfluorescein to hyaluronan/polylysine multilayers, ACS Appl. Mater. Int. 9 (2017) 38908–38918.
[46] M. Zhao, G. Altankov, U. Grabiec, M. Bennett, M. Salmeron-Sanchez, F. Dehghani, T. Groth, Molecular composition of GAG-collagen I multilayers affects remodeling of terminal layers and osteogenic differentiation of adipose-derived stem cells, Acta Biomater. 41 (2016) 86–99.
[47] M. Zhao, L. Li, C. Zhou, F. Heyroth, B. Fuhrmann, K. Maeder, T. Groth, Improved stability and cell response by intrinsic cross-linking of multilayers from collagen I and oxidized glycosaminoglycans, Biomacromolecules 15 (2014) 4272–4280.
[48] O. Svensson, T. Arnebrant, Mucin layers and multilayers — physicochemical properties and applications, Curr. Opin. Colloid Interface Sci. 15 (2010) 395–405.
[49] Caldwell Shi, Mucin adsorption to hydrophobic surfaces, J. Colloid Interface Sci. 224 (2000) 372–381.
[50] O. Svensson, L. Lindh, M. Cárdenas, T. Arnebrant, Layer-by-layer assembly of mucin and chitosan–influence of surface properties, concentration and type of mucin, J. Colloid Interface Sci. 299 (2006) 608–616.
[51] Y.A. Albarkah, R.J. Green, V.V. Khutoryanskiy, Probing the mucoadhesive interactions between porcine gastric mucin and some water-soluble polymers, Macromol. Biosci. 15 (2015) 1546–1553.
[52] T.V. Vakhrusheva, Y.P. Baikova, N.G. Balabushevich, S.A. Gusev, G.Y. Lomakina, E.A. Sholina, M.A. Moshkovskaya, P.L. Shcherbakov, O.V. Pobeguts, E.V. Mikhal'chik, Binding of mucin by E. coli from human gut, Bull. Exp. Biol. Med. 165 (2018) 235–238.
[53] L. Largitte, R. Pasquier, A review of the kinetics adsorption models and their application to the adsorption of lead by an activated carbon, Chem. Eng. Res. Des. 109 (2016) 495–504.
[54] A.I. Petrov, D.V. Volodkin, G.B. Sukhorukov, Protein-calcium carbonate coprecipitation: a tool for protein encapsulation, Biotechnol. Prog. 21 (2005) 918–925.
[55] J.M. Burchell, R. Beatson, R. Graham, J. Taylor-Papadimitriou, V. Tajadura-Ortega, O-linked mucin-type glycosylation in breast cancer, Biochem. Soc. Trans. 46 (2018) 779–788.
[56] Y. Svenskaya, B. Parakhonskiy, A. Haase, V. Atkin, E. Lukyanets, D. Gorin, R. Antolini, Anticancer drug delivery system based on calcium carbonate particles loaded with a photosensitizer, Biophys. Chem. 182 (2013) 11–15.
[57] C.E. Wagner, B.S. Turner, M. Rubinstein, G.H. McKinley, K. Ribbeck, A rheological study of the association and dynamics of MUC5AC gels, Biomacromolecules 18 (2017) 3654–3664.
[58] R. Bansil, J.P. Celli, J.M. Hardcastle, B.S. Turner, The influence of mucus microstructure and rheology in helicobacter pylori infection, Front. Immunol. 4 (2013) 310.
[59] D. Snary, A. Allen, R.H. Pain, The structure of pig gastric mucus conformational transitions induced by salt, Eur. J. Biochem. 24 (1971) 183–189.
[60] S.K. Lai, Y.-Y. Wang, J. Hanes, Mucus-penetrating nanoparticles for drug and gene delivery to mucosal tissues, Adv. Drug Deliv. Rev. 61 (2009) 158–171.
[61] G.L. Ellman, Tissue sulfhydryl groups, Arch. Biochem. Biophys. 82 (1959) 70–77.
[62] N.G. Balabushevich, A.V. Lopez de Guerenu, N.A. Feoktistova, A.G. Skirtach, D. Volodkin, Protein-containing multilayer capsules by templating on mesoporous $CaCO_3$ particles: POST- and PRE-loading approaches, Macromol. Biosci. 16 (2016) 95–105.
[63] J. Ahn, T. Crouzier, K. Ribbeck, M.F. Rubner, R.E. Cohen, Tuning the properties of mucin via layer-by-layer assembly, Biomacromolecules 16 (2015) 228–235.
[64] A. Dedinaite, M. Lundin, L. Macakova, T. Auletta, Mucin-chitosan complexes at the solid-liquid interface: multilayer formation and stability in surfactant solutions, Langmuir 21 (2005) 9502–9509.
[65] L. Lindh, I.E. Svendsen, O. Svensson, M. Cárdenas, T. Arnebrant, The salivary mucin MUC5B and lactoperoxidase can be used for layer-by-layer film formation, J. Colloid Interface Sci. 310 (2007) 74–82.
[66] S. Roy, K. Pal, A. Anis, K. Pramanik, B. Prabhakar, Polymers in mucoadhesive drug-delivery systems: a brief note, Des. Monomers Polym. 12 (2012) 483–495.
[67] E.D.H. Mansfield, K. Sillence, P. Hole, A.C. Williams, V.V. Khutoryanskiy, POZylation: a new approach to enhance nanoparticle diffusion through mucosal barriers, Nanoscale 7 (2015) 13671–13679.
[68] J.M. Laparra, Y. Sanz, Comparison of in vitro models to study bacterial adhesion to the intestinal epithelium, Lett. Appl. Microbiol. 49 (2009) 695–701.